

1 **Title:** Zoonotic potential of a novel bat morbillivirus

2 **Authors**

3 Satoshi Ikegame<sup>1</sup>, Jillian C. Carmichael<sup>1</sup>, Heather Wells<sup>2</sup>, Robert L. Furler<sup>3</sup>, Joshua A. Acklin<sup>1</sup>, Hsin-Ping  
4 Chiu<sup>1</sup>, Kasopefoluwa Y. Oguntuyo<sup>1</sup>, Robert M. Cox<sup>4</sup>, Aum R. Patel<sup>1</sup>, Shreyas Kowdle<sup>1</sup>, Christian S.  
5 Stevens<sup>1</sup>, Miles Eckley<sup>7</sup>, Shijun Zhan<sup>7</sup>, Jean K. Lim<sup>1</sup>, Takao Hashiguchi<sup>5</sup>, Edison Durigon<sup>6</sup>, Tony Schountz<sup>7</sup>,  
6 Jonathan E. Epstein<sup>8</sup>, Richard K. Plemper<sup>4</sup>, Peter Daszak<sup>8</sup>, Simon J. Anthony<sup>9</sup>, Benhur Lee<sup>1\*</sup>

7 **Affiliations**

8 1. Department of Microbiology at the Icahn School of Medicine at Mount Sinai, New York, NY  
9 2. Department of Ecology, Evolution and Environmental Biology, Columbia university, New York, NY  
10 3. Department of Medicine, Division of Infectious Diseases, Weill Cornell Medicine, New York, NY  
11 4. Institute for Biomedical Sciences, Georgia State University, Atlanta, GA  
12 5. Laboratory of Medical virology, Institute for Frontier Life and Medical Sciences, Kyoto University, Japan  
13 de Microbiologia, Instituto de Ciências Biomédicas, Universidade de São Paulo, Brazil  
14 7. Center for Vector-borne Infectious Diseases Department of Microbiology, Immunology and Pathology  
15 College of Veterinary Medicine Colorado State University  
16 8. EcoHealth Alliance, New York, NY  
17 9. Department of Pathology, Microbiology, and Immunology, UC Davis School of Veterinary Medicine

18 \* Correspondence to: [benhur.lee@mssm.edu](mailto:benhur.lee@mssm.edu) and [sjanthony@ucdavis.edu](mailto:sjanthony@ucdavis.edu).

19 **Competing interests:** All authors declare no competing interests.

20  
21 **Abstract**

22 Bats are significant reservoir hosts for many viruses with zoonotic potential<sup>1</sup>. SARS-CoV-2, Ebola virus,  
23 and Nipah virus are examples of such viruses that have caused deadly epidemics and pandemics when  
24 spilled over from bats into human and animal populations<sup>2,3</sup>. Careful surveillance of viruses in bats is critical  
25 for identifying potential zoonotic pathogens. However, metagenomic surveys in bats often do not result in  
26 full-length viral sequences that can be used to regenerate such viruses for targeted characterization<sup>4</sup>. Here,  
27 we identify and characterize a novel morbillivirus from a vespertilionid bat species (*Myotis riparius*) in  
28 Brazil, which we term myotis bat morbillivirus (MBaMV). There are 7 species of morbilliviruses including  
29 measles virus (MeV), canine distemper virus (CDV) and rinderpest virus (RPV)<sup>5</sup>. All morbilliviruses cause  
30 severe disease in their natural hosts<sup>6-10</sup>, and pathogenicity is largely determined by species specific  
31 expression of canonical morbillivirus receptors, CD150/SLAMF1<sup>11</sup> and NECTIN4<sup>12</sup>. MBaMV used *Myotis*  
32 *spp* CD150 much better than human and dog CD150 in fusion assays. We confirmed this using live MBaMV  
33 that was rescued by reverse genetics. Surprisingly, MBaMV replicated efficiently in primary human  
34 myeloid but not lymphoid cells. Furthermore, MBaMV replicated in human epithelial cells and used human  
35 NECTIN4 almost as well as MeV. Our results demonstrate the unusual ability of MBaMV to infect and  
36 replicate in some human cells that are critical for MeV pathogenesis and transmission. This raises the  
37 specter of zoonotic transmission of a bat morbillivirus.

## 38 **Results**

39 **Isolation of MBaMV sequence.** During a metagenomic genomic survey of viruses in bats, we identified  
40 a full-length morbillivirus sequence from a riparian myotis bat (*Myotis riparius*) in Brazil. This myotis bat  
41 morbillivirus (MBaMV) had a genome length of 15,804 nucleotides consistent with the rule of six and  
42 comprise of six transcriptional units encoding the canonical open reading frames (ORFs) of nucleo (N)  
43 protein, phospho (P) protein, matrix (M) protein, fusion (F) protein, receptor binding protein (RBP), and  
44 large (L) protein (Extended Data Fig. 1a). The sizes of these ORFs are comparable to their counterparts in  
45 the other morbilliviruses (Extended Data Fig. 1b). Phylogenetic analysis using the full-length L protein  
46 sequence indicated that MBaMV is most closely related to canine distemper virus (CDV) and phocine  
47 distemper virus (PDV) (Extended Data Fig. 1c, Extended Data Table 1).

48 Paramyxovirus proteins with the most frequent and direct interactions with host proteins, such as P and its  
49 accessory gene products (V and C) as well as the RBP, tend to exhibit the greatest diversity<sup>13</sup>. Morbillivirus  
50 P, V and C antagonize host-specific innate immune responses while its RBP interacts with host-specific  
51 receptors. That these proteins are under evolutionary pressure to interact with different host proteins is  
52 reflected in the lower conservation of MBaMV P/V/C (31-43%) and RBP (27-32%) with other morbillivirus  
53 homologs. This is in contrast to the relatively high conservation (52-76%) of MBaMV N, M, F, and L  
54 proteins with their respective morbillivirus counterparts (Extended Data Fig. 2).

55  
56 **Species specific receptor usage.** The use of CD150/SLAMF1 to enter myeloid and lymphoid cells is a  
57 hallmark of morbilliviruses, and also a major determinant of pathogenicity. CD150 is highly divergent  
58 across species, and accounts for the species restricted tropism of most morbilliviruses<sup>14</sup>. Thus, we first  
59 characterized the species-specific receptor tropism of MBaMV. We performed a quantitative image-based  
60 fusion assay (QIFA) by co-transfecting expression vectors encoding MBaMV-F and -RBP, along with  
61 CD150 from the indicated species into receptor-negative CHO cells. MeV-RBP and F formed more  
62 syncytia in CHO cells upon human-CD150 (hCD150) co-transfection compared to dog-CD150 (dCD150)  
63 or bat-CD150 (bCD150) (Fig. 1a, top row). In contrast, MBaMV-RBP and F formed bigger and more

64 numerous syncytia upon bCD150 overexpression than hCD150 or dCD150 (Fig. 1a, middle row). CDV-  
65 RBP and F formed extensive syncytia with both dCD150 and bCD150, and moderate syncytia with hCD150  
66 and even mock-transfected cells (Fig. 1a, bottom row), suggesting a degree of promiscuity. We quantified  
67 these differential syncytia formation results on an image cytometer as described<sup>15</sup> (Fig. 1b).  
68 We also evaluated the receptor usage of MBaMV in a VSV-pseudotype entry assay. VSV-ΔG[Rluc] bearing  
69 MeV-RBP and F entered hCD150-transfected CHO cells better than dCD150-, bCD150-, or mock-  
70 transfected cells (Fig. 1c) as expected. MBaMV-pseudotypes entered only bCD150-transfected CHO cells.  
71 CDV-pseudotypes showed good entry into dCD150- and bCD150-transfected, but not hCD150-transfected  
72 CHO cells. These results are generally consistent with our fusion assay results and support the species  
73 specificity of morbilliviruses. The promiscuity of CDV RBP for bCD150 suggest potential for epizoonotic  
74 transmissions from carnivores into some chiropteran species.

75

76 **Generation of MBaMV by reverse genetics.** Next, we attempted to generate a genomic cDNA clone of  
77 MBaMV that we could rescue by reverse genetics. We synthesized and assembled the putative MBaMV  
78 genome in increasingly larger fragments. Two silent mutations were introduced in the N-terminal 1.5 kb  
79 of the L gene to disrupt a cryptic open reading frame (Extended Data Fig. 3) that initially prevented cloning  
80 of the entire MBaMV genome. We introduced an additional EGFP transcription unit at the 3' terminus and  
81 rescued this MBaMV-GFP genome using the N, P, and L accessory plasmid from MeV (Extended Data Fig.  
82 1a). MBaMV-GFP was initially rescued in BSR-T7 cells but passaged, amplified, and titered on Vero-  
83 bCD150 cells (Extended Data Fig. 4a). MBaMV formed GFP-positive syncytia containing hundreds of  
84 nuclei at 3 days post-infection (dpi) (Fig. 2a) and relatively homogenous plaques by 7 dpi (Fig. 2b).  
85 Transmission electron microscopy (TEM) (Fig. 2c) captured numerous virions budding from Vero-bCD150  
86 cells with pleiomorphic structure and size (~100-200 nm) consistent with paramyxovirus particles. At high  
87 magnification, virions were outlined by protrusions suggestive of surface glycoproteins. RNP-like  
88 structures can be found in the interior of the virion shown. These observations are consistent with previous  
89 findings from MeV<sup>16</sup>.

90

91 **Evaluation of receptor usage by MBaMV.** To understand how well CD150 from various hosts supports  
92 MBaMV replication, we tested MBaMV growth in parental Vero-CCL81 cells and isogenic derivatives  
93 constitutively expressing CD150 of human, dog, or bat. MBaMV formed huge syncytia (Fig 3a) at 2 dpi in  
94 Vero-bCD150 cells and reached peak titers of  $\sim 10^5$  PFU/ml at 3 dpi (Fig 3b). MBaMV showed moderate  
95 syncytia spread and growth in Vero-dCD150 cells but peak titers at 5 dpi was  $\sim 100$ -fold lower. No  
96 significant virus growth was detected in Vero or Vero-hCD150 cells. These results confirm that MBaMV  
97 can use bCD150 but not hCD150 for efficient cell entry and replication. MBaMV appears to use dCD150,  
98 albeit to a much lesser extent than bCD150.

99 MeV uses human nectin-4 as the epithelial cell receptor<sup>17,18</sup> which mediates efficient virus shedding from  
100 the affected host<sup>12,19</sup>. CDV also uses human nectin-4 efficiently for entry and growth<sup>20</sup>. To test if MBaMV  
101 can use human nectin-4 in an epithelial cell context, we evaluated the replication kinetics of MBaMV in  
102 human lung epithelial cells that express high (H441) or low (A549) levels of nectin-4<sup>12,21</sup>(Extended Data  
103 Fig. 4b). Surprisingly, MBaMV showed efficient virus spread (Fig. 3c) in H441 cells and reached  $10^4$   
104 PFU/ml by 6 dpi (Fig. 3d). In contrast, MBaMV showed small GFP foci and 10 times lower titer in A549  
105 cells. Comparing the Area Under Curve (AUC) revealed significant differences in this growth curve metric  
106 (Fig. 3e). However, MeV still replicated to higher titers than MBaMV in H441 cells (Fig. 3d-e). This could  
107 be due to species specific host factors or differences in interferon antagonism between human and bat  
108 morbilliviruses. Thus, we tested MBaMV versus MeV growth in interferon-defective Vero-human nectin-  
109 4 cells (Vero-hN4). MBaMV and MeV replicated and spread equally well on Vero-hN4 cells (Fig 3f-g),  
110 validating the ability of MBaMV to use human nectin-4, and suggesting that MBaMV may not have fully  
111 adapted to counteracting human innate immune responses.

112

113 **Molecular characterization of MBaMV.** To better understand the transcriptional profile of MBaMV, we  
114 used Nanopore long-read direct RNA sequencing to sequence the mRNAs of MBaMV-infected Vero-  
115 bCD150 cells at 2 dpi (MOI=0.01). We found a characteristic 3'- 5' transcriptional gradient where

116 GFP>N>P>M>F>RBP>L (Extended Data Fig. 5a). Morbilliviruses have a conserved intergenic motif  
117 (CUU) between the gene end and gene start of adjacent genes ‘AAAA-CUU-AGG’. This intergenic motif  
118 was not immediately apparent in the long complex M-F intergenic region of the assembled MBaMV  
119 genome. However, the high coverage of this M-F intergenic region (M read-through transcripts) identified  
120 the M-F intergenic motif as ‘CGU’ instead of ‘CUU’ (Extended Data Fig. 5b).

121 The P gene of morbilliviruses is known to generate the V or W genes through the insertion of one or two  
122 guanines, respectively, at the conserved editing motif (AAAAGGG)<sup>22</sup>, which is present in MBaMV.  
123 Amplicon sequencing of the P gene editing motif—from the same mRNA pool used above—revealed the  
124 frequency of P, V, and W mRNA is 42.1%, 51.2%, and 2.6%, respectively (Extended Data Fig. 5c),  
125 suggesting that the major interferon antagonist (V) is produced even in the absence of interferon.

126 We next evaluated the expression and cleavage of two surface glycoproteins (RBP and F). C-terminal AU-  
127 1 tagged F construct showed uncleaved F0 and cleaved F1 (Extended Data Fig. 5d). C-terminal HA tagged  
128 RBP construct showed monomer in addition to oligomers (Extended Data Fig. 5e). MBaMV-RBP showed  
129 smear above 110 kDa which is suggestive of oligomerization even in the reducing condition.

130

131 **Species tropism of MBaMV.** The two suborders of chiropterans (bats), Pteropodiformes  
132 (Yinpterochiroptera) and Vespertilioniformes (Yangochiroptera), include more than 1,400 species grouped  
133 into 6 and 14 families, respectively<sup>23</sup>. Myotis bats belong to the prototypical Vespertilionidae family that is  
134 the namesake of its suborder. Jamaican fruit bats belong to the same suborder as myotis bats, albeit from a  
135 different family (Phyllostomidae). We inoculated 6 Jamaican fruit bats (*Artibeus jamaicensis*) available in  
136 a captive colony via two different routes with MbaMV to assess its pathogenicity *in vivo*. All bats remained  
137 asymptomatic and showed no evidence of developing systemic disease up to 3 weeks post-infection. Nor  
138 could we detect any molecular or serological evidence of productive infection (Extended Data Fig. 6).  
139 Inspection of Jamaican fruit bat and myotis CD150 sequences revealed key differences in the predicted  
140 contact surfaces with RBP (discussed below), which we speculate are responsible for the species-specific  
141 restriction seen in our experimental challenge of Jamaican fruit bats with MBaMV.

142 To identify RBP-CD150 interactions likely involved in determining host species tropism, we compared the  
143 amino acid sequences at the putative contact surfaces of morbillivirus RBPs and their cognate CD150  
144 receptors. Using PDBePISA<sup>24</sup>, we identified three key regions in MeV-RBP (residues 188-198, 498-507,  
145 and 524-556, Extended Data Fig. 7a-c) occluding two regions in CD150 (residues 60-92 and 119-131 of  
146 human CD150, Extended Data Fig. 8) in the crystal structure of MeV-RBP bound to CD150 (PDB ID:  
147 3ALW)<sup>25</sup>. Alignment of key regions in morbillivirus RBPs implicated in CD150 interactions reveals virus-  
148 specific differences that suggest adaptation of morbillivirus RBPs to the CD150 receptors of their natural  
149 host. Most notably, MBaMV lacks the DxD motif at residues 501-503 (505-507 in MeV) that is present in  
150 all morbilliviruses except FeMV (Extended Data Fig. 7). These residues form multiple salt bridges and  
151 hydrogen bonds that stabilize MeV-RBP and hCD150 interactions. Their conservation suggest they perform  
152 similar roles for other morbilliviruses. On the CD150 side (Extended Data Fig. 8), residues 70-76 and 119-  
153 126 are the most variable between host species. Interestingly, Jamaican fruit bat and *Myotis* CD150 differ  
154 considerably in these regions, providing a rationale for the non-productive infection we saw in our Jamaican  
155 fruit bat challenge experiments.

156

### 157 **Susceptibility of human myeloid and lymphoid cells to MBaMV.**

158 Alveolar macrophages and activated T- and B-cells expressing CD150 are the initial targets for measles  
159 virus entry and systemic spread. To better assess the zoonotic risks posed by MBaMV, we compared how  
160 well human and bat morbilliviruses can infect human monocyte-derived macrophages (MDMs) and  
161 peripheral blood mononuclear cells (PBMCs). Both MeV and MBaMV infected MDMs were clearly GFP+  
162 24 hpi (Fig. 4a), but infection was variable between donors and even between different viral stocks on the  
163 same donor (Fig. 4b). However, MeV infection of MDMs was inhibited by sCD150 whereas MBaMV  
164 infections were not (Fig. 4c). Interestingly, MeV infection led to an apparent downregulation of CD150 as  
165 expected<sup>26</sup> (Fig. 4d, GFP-high/CD150-negative R3 gate), whereas MBaMV infection led to a GFP-dim  
166 population with variable CD150 expression on occasions where infection was high enough for such  
167 evaluation (Fig. 4d, R2 gate). Conversely, when PBMCs were stimulated with concanavalin A and IL-2,

168 only MeV robustly infected these cells (Fig. 4e).

169

### 170 **MBaMV is sensitive to morbillivirus RNA dependent RNA polymerase inhibitors**

171 Potential drug treatments are a critical issue for emerging viruses. Thus, we tested if MBaMV is susceptible  
172 to currently available drugs. We have developed two orally bioavailable small compounds targeting the L  
173 protein of morbilliviruses, GHP-88309<sup>27</sup> and ERDRP-0519<sup>28</sup>. The differences between MeV and MBaMV  
174 across the five functional domains of the L protein are shown schematically in Extended Data Fig. 9a<sup>29</sup>. *In*  
175 *silico* modelling (Extended Data Fig. 9b) predicts that both drugs should bind similarly to MeV and  
176 MBaMV L protein. Closer inspection of the ERDRP-0519 binding pocket (Extended Data Fig. 9c) shows  
177 1155-1158 YGLE and H1288 residues interacting with ERDRP-0519. These residues directly interact with  
178 ERDRP-0519 in MeV L<sup>30</sup>. Modeling of the GHP-88309 binding pocket (Extended Data Fig. S9d) reveals  
179 involvement of E863, S869, Y942, I1009, and Y1105 residues which were previously reported as escape  
180 mutants of GHP-88309 in MeV<sup>27</sup>. As predicted, both drugs inhibited MBaMV growth in dose dependent  
181 manner (Extended Data Fig 9e and f). Although the EC<sub>50</sub> of GHP-88309 is lower for MeV than MBaMV,  
182 (0.6 μM and 3.0 μM, respectively), GHP-88309 reaches a plasma concentration of >30 μM in animal  
183 models, indicating this drug could be an effective MBaMV *in vivo*.

### 184 **Discussion**

185 Metagenomic viral surveillance studies aided by next-generation sequencing have allowed scientists to  
186 monitor viruses circulating in animal species and identify potential zoonotic threats<sup>31</sup>. Surveillance of bat  
187 species has been particularly critical. For instance, >60 novel paramyxovirus sequences were identified in  
188 a 2012 bat surveillance study, several of which mapped to the Morbillivirus genus<sup>4</sup>. While comparing novel  
189 virus sequences to known pathogens may help inform the risks associated with future spillover events, this  
190 type of *in silico* modeling based on incomplete viral sequences needs to be complemented by functional  
191 characterization of such viruses. In this study, we identified a full-length morbillivirus genomic sequence  
192 from *Myotis riparius* bats in Brazil and generated an infectious virus clone using reverse genetics. With this  
193 approach, we circumvented the arduous process of isolating and culturing live virus directly from animals

194 and instead produced MBaMV in the lab.

### 195 **MBaMV characterized as a morbillivirus**

196 Prior to this study, there were only 7 ICTV recognized morbilliviruses species, none of which were isolated  
197 from bats. While the annotated MBaMV genome aligned with the classic morbillivirus genome organization  
198 (N, P/V/C, M, F, RBP, and L), it was important to verify that virus generated by reverse genetics  
199 successfully recapitulated morbillivirus biology. Fusion assays and entry experiments confirmed that  
200 MBaMV preferentially used myotis CD150 over human or dog CD150 to enter transgenic Vero cells (Fig.  
201 3), which fits the paradigm that CD150 is the major determinant of host specificity for morbilliviruses. We  
202 also assessed P-editing—a hallmark of paramyxoviruses—and found RNA editing of P-mRNA, creating V-  
203 mRNA (single G insertion) or W-mRNA (double G insertion) of MBaMV. Interestingly, the proportion of  
204 V-mRNA at 51.2% of total P transcripts is unusually high for orthoparamyxoviruses, resembling the now  
205 extinct rinderpest virus (RPV) more than extant morbilliviruses<sup>32</sup>.

206 In their natural hosts, morbillivirus are highly pathogenic and can cause deadly acute infections<sup>33</sup>. Thus, a  
207 reasonable prediction is that MBaMV would cause visible disease in the bat host. However, when we  
208 challenged Jamaican fruit bats with MBaMV, we found the virus was *not* able to cause systemic disease in  
209 the bats (Extended Data Fig. 6) and there was no evidence that MBaMV productively infected these bats.  
210 This lack of infection is likely due to the CD150 differences between the species—CD150 of Jamaican fruit  
211 bats and *Myotis* species is only 70% conserved on the amino acid level (Extended Fig. 8). We predict that  
212 MBaMV infection is much more likely to cause serious disease in the *Myotis riparius* species.

### 213 **Potential zoonotic threat of MBaMV based on receptor usage**

214 While non-human morbilliviruses are not currently known to jump the species barrier and infect humans,  
215 we did find that MBaMV was able to utilize human receptors *in vitro* to a certain extent. Notably, MBaMV  
216 replicated well in H441 cells and in Vero cells expressing human nectin-4 (Fig. 3). CDV is also reported to  
217 use human nectin-4<sup>20</sup> and can replicate in H358 cells<sup>34</sup>. Alarmingly, there have been several outbreaks of  
218 CDV in non-human primates, resulting in acute disease or death in the animals<sup>35</sup>. In one outbreak, mutations  
219 were found in the RBP which rendered CDV-RBP capable of efficiently using primate-CD150<sup>20</sup>. However,



220 CDV is unlikely to adapt to humans in the presence of cross-reactive MeV immunity. Whether such cross-  
221 reactivity extends to MBaMV remains to be seen. Traditionally, morbilliviruses use CD150 to enter myeloid  
222 and lymphoid cells. However, unlike MeV which infects human macrophages via CD150, MBaMV infects  
223 human macrophages in a CD150-independent manner (Fig. 4c)<sup>36</sup>. This result indicates that a non-  
224 CD150/nectin-4 entry receptor for MBaMV exists on human macrophages. Whether or not this unidentified  
225 receptor would allow for pathogenicity of MBaMV in a human host is yet to be determined.

226

227

228

229

230

231

232

233

234

235

236

237

238

239

240

241

242

243

244

245

## 246 References

- 247 1. Wang, L. F. & Anderson, D. E. Viruses in bats and potential spillover to animals and humans. *Curr.*  
248 *Opin. Virol.* **34**, 79–89 (2019).
- 249 2. Han, H. J. *et al.* Bats as reservoirs of severe emerging infectious diseases. *Virus Res.* **205**, 1–6 (2015).
- 250 3. Letko, M., Seifert, S. N., Olival, K. J., Plowright, R. K. & Munster, V. J. Bat-borne virus diversity,  
251 spillover and emergence. *Nat. Rev. Microbiol.* **18**, (2020).
- 252 4. Felix Drexler, J. *et al.* Bats host major mammalian paramyxoviruses. *Nat. Commun.* **3**, (2012).
- 253 5. Amarasinghe, G. K. *et al.* Taxonomy of the order Mononegavirales: update 2017. **162**, 2493–2504  
254 (2017).
- 255 6. Morens, D. M., Holmes, E. C., Davis, A. S. & Taubenberger, J. K. Global Rinderpest Eradication:  
256 Lessons Learned and Why Humans Should Celebrate Too. *J. Infect. Dis.* **204**, 502 (2011).
- 257 7. Donduashvili, M. *et al.* Identification of Peste des Petits Ruminants Virus, Georgia, 2016. *Emerg.*  
258 *Infect. Dis.* **24**, 1576 (2018).
- 259 8. Beineke, A., Puff, C., Seehusen, F. & Baumgärtner, W. Pathogenesis and immunopathology of  
260 systemic and nervous canine distemper. *Vet. Immunol. Immunopathol.* **127**, 1–18 (2009).
- 261 9. Couacy-Hymann, E., Bodjo, C., Danho, T., Libeau, G. & Diallo, A. Evaluation of the virulence of  
262 some strains of peste-des-petits-ruminants virus (PPRV) in experimentally infected West African  
263 dwarf goats. *Vet. J.* **173**, 178–183 (2007).
- 264 10. Bressemer, M.-F. Van *et al.* Cetacean Morbillivirus: Current Knowledge and Future Directions.  
265 *Viruses* **6**, 5145 (2014).
- 266 11. Tatsuo, H., Ono, N., Tanaka, K. & Yanagi, Y. SLAM (CDw150) is a cellular receptor for measles  
267 virus. *Nature* **406**, 893–897 (2000).
- 268 12. Mühlebach, M. *et al.* Adherens junction protein nectin-4 is the epithelial receptor for measles virus.  
269 *Nature* **480**, 530–533 (2011).
- 270 13. Thibault, P. A., Watkinson, R. E., Moreira-Soto, A., Drexler, J. F. & Lee, B. Zoonotic potential of  
271 emerging paramyxoviruses: knowns and unknowns. *Adv. Virus Res.* **98**, 1 (2017).
- 272 14. Ohishi, K., Maruyama, T., Seki, F. & Takeda, M. Marine Morbilliviruses: Diversity and Interaction  
273 with Signaling Lymphocyte Activation Molecules. *Viruses* **11**, (2019).
- 274 15. Ikegame, S. *et al.* Fitness selection of hyperfusogenic measles virus F proteins associated with  
275 neuropathogenic phenotypes. *Proc. Natl. Acad. Sci. U. S. A.* **118**, (2021).
- 276 16. Nakai, M. & Imagawa, D. T. Electron Microscopy of Measles Virus Replication. *J. Virol.* **3**, 187  
277 (1969).
- 278 17. Mateo, M., Navaratnarajah, C. K. & Cattaneo, R. Structural basis of efficient contagion: measles  
279 variations on a theme by parainfluenza viruses. *Curr. Opin. Virol.* **0**, 16 (2014).

- 280 18. Lin, L. T. & Richardson, C. D. The host cell receptors for measles virus and their interaction with  
281 the viral Hemagglutinin (H) Protein. *Viruses* **8**, 1–29 (2016).
- 282 19. Leonard, V. *et al.* Measles virus blind to its epithelial cell receptor remains virulent in rhesus  
283 monkeys but cannot cross the airway epithelium and is not shed. *J. Clin. Invest.* **118**, (2008).
- 284 20. Sakai, K. *et al.* Lethal canine distemper virus outbreak in cynomolgus monkeys in Japan in 2008. *J.*  
285 *Viol.* **87**, 1105–1114 (2013).
- 286 21. Noyce, R. S. *et al.* Tumor Cell Marker PVRL4 (Nectin 4) Is an Epithelial Cell Receptor for Measles  
287 Virus. *PLoS Pathog.* **7**, (2011).
- 288 22. Cattaneo, R., Kaelin, K., Baczko, K. & Billeter, M. A. Measles virus editing provides an additional  
289 cysteine-rich protein. *Cell* **56**, 759–764 (1989).
- 290 23. Eick, G. N., Jacobs, D. S. & Matthee, C. A. A nuclear DNA phylogenetic perspective on the  
291 evolution of echolocation and historical biogeography of extant bats (Chiroptera). *Mol. Biol. Evol.*  
292 **22**, 1869–1886 (2005).
- 293 24. Krissinel, E. & Henrick, K. Inference of Macromolecular Assemblies from Crystalline State. *J. Mol.*  
294 *Biol.* **372**, 774–797 (2007).
- 295 25. Hashiguchi, T. *et al.* Structure of the measles virus hemagglutinin bound to its cellular receptor  
296 SLAM. *Nat. Struct. Mol. Biol.* **18**, 135–142 (2011).
- 297 26. Welstead, G. G., Hsu, E. C., Iorio, C., Bolotin, S. & Richardson, C. D. Mechanism of CD150  
298 (SLAM) Down Regulation from the Host Cell Surface by Measles Virus Hemagglutinin Protein. *J.*  
299 *Viol.* **78**, 9666–9674 (2004).
- 300 27. Cox, R. M. *et al.* Orally efficacious broad-spectrum allosteric inhibitor of paramyxovirus  
301 polymerase. *Nat. Microbiol.* **5**, 1232–1246 (2020).
- 302 28. Krumm, S. A. *et al.* An orally available, small-molecule polymerase inhibitor shows efficacy against  
303 a lethal morbillivirus infection in a large animal model. *Sci. Transl. Med.* **6**, 1–11 (2014).
- 304 29. Abdella, R., Aggarwal, M., Okura, T., Lamb, R. A. & He, Y. Structure of a paramyxovirus  
305 polymerase complex reveals a unique methyltransferase-CTD conformation. *Proc. Natl. Acad. Sci.*  
306 *U. S. A.* **117**, 4931–4941 (2020).
- 307 30. Cox, R. M., Sourimant, J., Govindarajan, M., Natchus, M. G. & Plemper, R. K. Therapeutic targeting  
308 of measles virus polymerase with ERDRP-0519 suppresses all RNA synthesis activity. *PLOS*  
309 *Pathog.* **17**, e1009371 (2021).
- 310 31. Li, B. *et al.* Discovery of Bat Coronaviruses through Surveillance and Probe Capture-Based Next-  
311 Generation Sequencing. *mSphere* **5**, 1–11 (2020).
- 312 32. Douglas, J., Drummond, A. J. & Kingston, R. L. Evolutionary history of cotranscriptional editing in  
313 the paramyxoviral phosphoprotein gene. *Virus Evol.* **7**, (2021).

- 314 33. De Vries, R. D., Paul Duprex, W. & De Swart, R. L. Morbillivirus infections: An introduction.  
315 *Viruses* **7**, 699–706 (2015).
- 316 34. Otsuki, N. *et al.* The V Protein of Canine Distemper Virus Is Required for Virus Replication in  
317 Human Epithelial Cells. *PLoS One* **8**, e82343 (2013).
- 318 35. Kennedy, J. M. *et al.* Canine and Phocine Distemper Viruses : Species Barriers. *Viruses* **11**, (2019).
- 319 36. Minagawa, H., Tanaka, K., Ono, N., Tatsuo, H. & Yanagi, Y. Induction of the measles virus receptor  
320 SLAM (CD150) on monocytes. *J. Gen. Virol.* **82**, 2913–2917 (2001).
- 321 37. Anthony, S. J. *et al.* Further evidence for bats as the evolutionary source of middle east respiratory  
322 syndrome coronavirus. *MBio* **8**, 1–13 (2017).
- 323 38. Kumar, S., Stecher, G., Li, M., Knyaz, C. & Tamura, K. MEGA X: Molecular evolutionary genetics  
324 analysis across computing platforms. *Mol. Biol. Evol.* **35**, 1547–1549 (2018).
- 325 39. Ono, N. *et al.* Measles Viruses on Throat Swabs from Measles Patients Use Signaling Lymphocytic  
326 Activation Molecule (CDw150) but Not CD46 as a Cellular Receptor. *J. Virol.* **75**, 4399–4401  
327 (2001).
- 328 40. Seki, F., Ono, N., Yamaguchi, R. & Yanagi, Y. Efficient Isolation of Wild Strains of Canine  
329 Distemper Virus in Vero Cells Expressing Canine SLAM (CD150) and Their Adaptability to  
330 Marmoset B95a Cells. *J. Virol.* **77**, 9943–9950 (2003).
- 331 41. Tatsuo, H., Ono, N. & Yanagi, Y. Morbilliviruses Use Signaling Lymphocyte Activation Molecules  
332 (CD150) as Cellular Receptors. *J. Virol.* **75**, 5842–5850 (2001).
- 333 42. Seki, F. *et al.* The SI Strain of Measles Virus Derived from a Patient with Subacute Sclerosing  
334 Panencephalitis Possesses Typical Genome Alterations and Unique Amino Acid Changes That  
335 Modulate Receptor Specificity and Reduce Membrane Fusion Activity. *J. Virol.* **85**, 11871 (2011).
- 336 43. von Messling, V., Zimmer, G., Herrler, G., Haas, L. & Cattaneo, R. The Hemagglutinin of Canine  
337 Distemper Virus Determines Tropism and Cytopathogenicity. *J. Virol.* **75**, 6418–6427 (2001).
- 338 44. Beaty, S. M. *et al.* Efficient and Robust Paramyxoviridae Reverse Genetics Systems . *mSphere* **2**,  
339 (2017).
- 340 45. Oguntuyo, K. Y. *et al.* Quantifying absolute neutralization titers against SARS-CoV-2 by a  
341 standardized virus neutralization assay allows for cross-cohort comparisons of COVID-19 sera.  
342 *MBio* **12**, 1–23 (2021).
- 343 46. Hashiguchi, T. *et al.* Crystal structure of measles virus hemagglutinin provides insight into effective  
344 vaccines. *Proc. Natl. Acad. Sci. U. S. A.* **104**, 19535–19540 (2007).
- 345 47. Waterhouse, A. *et al.* SWISS-MODEL: Homology modelling of protein structures and complexes.  
346 *Nucleic Acids Res.* **46**, W296–W303 (2018).
- 347 48. Madeira, F. *et al.* The EMBL-EBI search and sequence analysis tools APIs in 2019. *Nucleic Acids*

- 348            *Res.* **47**, W636–W641 (2019).
- 349    49.    Pei, J. & Grishin, N. V. AL2CO: Calculation of positional conservation in a protein sequence  
350            alignment. *Bioinformatics* **17**, 700–712 (2001).
- 351    50.    Noda, T. *et al.* Importance of the 1+7 configuration of ribonucleoprotein complexes for influenza A  
352            virus genome packaging. *Nat. Commun.* **9**, 1–10 (2018).

353

354

355

356

357

358

359

360

361

362

363

364

365

366

367

368

369

370

371

372

373

374

375

376

377

378

379

380

381

## 382 **Materials and methods**

### 383 **Method to isolate bat morbillivirus sequence**

384 The bat surveillance was conducted in the Amazon region of Brazil. The bat was a subadult male (immature,  
385 but independent) and apparently healthy. Mitochondrial DNA profiling (MW554523 and MW557650)  
386 identified bat as a riparian myotis (*Myotis riparius*). RNA was subjected to NGS analysis, and viral genome  
387 (MW557651) was assembled from fastq read files (GSE166170). The bat was captured by mist net, then  
388 oral, rectal, and urogenital swabs were all collected for RNA extraction. Total nucleic acid (TNA) was  
389 extracted using the Roche MagNA Pure 96 platform following the manufacturer's protocol, then TNA was  
390 DNase treated (DNase I; Ambion, Life Technologies, Inc.) and reverse transcribed using SuperScript III  
391 (Invitrogen, Life Technologies, Inc.) with random hexamer primers. The cDNA was treated with RNase H  
392 before second-strand synthesis by Klenow fragment (3' to 5' exonuclease) (New England Biolabs), then the  
393 double-stranded cDNA was sheared into average of 200 bps fragments using a Covaris focused  
394 ultrasonicator E210. Sheared cDNA was deep sequenced using the Illumina HiSeq 2500 platform and reads  
395 were bioinformatically de novo assembled using MEGAHIT v1.2.8 after quality control steps and exclusion  
396 of host reads using Bowtie2 v2.3.5<sup>37</sup>. This method was same as previously published. The virus was  
397 identified in the rectal swab.

398

### 399 **Generation of phylogenetic tree and conservation matrix table**

400 Amino acid sequences of L proteins were aligned by ClustalW, then the evolutionary history of L proteins  
401 was inferred by Maximum Likelihood method with bootstrap test of 1,000 replicates. All processes were  
402 done in MEGA X<sup>38</sup>. For conservation matrix table, amino acid sequences of each gene were aligned by  
403 ClustalW, then the conservations were evaluated. The accession numbers used for the alignment were  
404 summarized in Table S1.

405

### 406 **Cells**

407 293T cells (ACTT Ca# CRL-3216), A549 cells (ATCC Ca# CCL-185), Vero cells (ATCC Cat# CCL-81,  
408 RRID:CVCL\_0059), and BSR T7/5 cells (RRID:CVCL\_RW96) were grown in in Dulbecco's modified  
409 Eagle's medium (DMEM, ThermoFisher Scientific, USA) supplemented with 10% fetal bovine serum  
410 (FBS, Atlanta Biologicals, USA) at 37°C. NCI-H441 cells (ATCC Ca# HTB-174) were grown in RPMI  
411 1640 medium (ThermoFisher Scientific, USA) with 10% FBS. Vero-hCD150 (Vero-human SLAM) cells  
412 are Vero cells derivative which constitutively express hCD150. Vero-dCD150 cells are Vero cells derivative  
413 which constitutively express HA-dCD150. Vero-hCD150 cells<sup>39</sup> and Vero-dCD150 cells<sup>40</sup> were provided  
414 by Dr. Yanagi at Kyushu University and maintained in DMEM with 10% FBS. Vero-bCD150 cells and  
415 Vero-human nectin-4 cells were generated as written below and maintained in DMEM with 10% FBS. CHO

416 cells were grown in DMEM/F12 (1:1) medium (gibco) with 10% FBS.

417

#### 418 **Plasmids**

419 We cloned the open reading frame of hCD150, dCD150, and bCD150 (from *Myostis brandtii*) into the  
420 pCAGGS vector cut by *EcoRI* (NEB) and *NheI*-HF (NEB). We introduced HA tag-linker-Igk signal  
421 peptides (amino acids corresponding to; MVLQTQVFISLLLWISGAYG-YPYDVPDYA-GAQPASP) at  
422 the N-terminus of CD150s as previously reported<sup>41</sup>. The sequence of hCD150, dCD150, bCD150 sequence  
423 were from NP\_003028.1, NP\_001003084.1, and XP\_014402801.1, respectively. We synthesized codon  
424 optimized gene sequences at GeneArt Gene Synthesis (Invitrogen), generating pCAGGS-Igk-HA-hCD150,  
425 pCAGGS-Igk-HA-dCD150, pCAGGS-Igk-HA-bCD150. We also generated pCAGGS-Igk-HA-bCD150-  
426 P2A-Puro which additionally express puromycin resistant gene. For pCAGGS-human nectin-4-P2A-puro,  
427 synthesized DNA by GeneArt Gene Synthesis (Invitrogen) was cloned into pCAGGS.

428 The sequence of MBaMV RBP and F open reading frame were synthesized by GenScript. These were  
429 cloned into pCAGGS vector cut by *EcoRI* and *NheI*-HF with adding HA tag (RBP gene) or AU1 tag (F  
430 gene) in C-terminus, generating pCAGGS-MBaMV-RBP-HA, pCAGGS-MBaMV-F-AU1.

431 For MeV RBP and F expressing plasmid, we amplified RBP and F sequence from p(+) MV323-AcGFP  
432 with the addition of HA-tag and AU1-tag same as MBaMV-RBP and -F, creating pCAGGS-MeV-RBP-HA,  
433 pCAGGS-MeV-F-AU1. For CDV RBP and F cloning, we amplified RBP and F sequence from pCDV-  
434 5804P plasmid with the addition of HA-tag and AU1-tag, creating pCAGGS-CDV-RBP-HA, pCAGGS-  
435 CDV-F-AU1.

436 Genome coding plasmids for MeV; (p(+) MV323-AcGFP) and CDV; pCDV-5804P were kindly gifted from  
437 Dr. Makoto Takeda<sup>42</sup> and Dr. Veronica von Messling respectively<sup>43</sup>. We transferred the MeV genome  
438 sequence into pEMC vector, adding an optimal T7 promoter, a hammer head ribozyme, and we introduced  
439 an eGFP transcriptional unit at the head of the genome (pEMC-IC323-eGFP), which is reported in the  
440 previous study<sup>15</sup>.

441 For the generation of MBaMV genome coding plasmid, we synthesized pieces of DNA at 2000 - 6000 bps  
442 at Genscript with the addition of eGFP transcriptional unit at the head of genome (eGFP-MBaMV). DNA  
443 fragments were assembled into pEMC vector one-by-one using in-fusion HD cloning kit (Takara),  
444 generating pEMC-eGFP-MBaMV. The N-terminal 1.5 kb of the L gene was initially unclonable. Sequence  
445 analysis revealed a putative 86 aa open reading frame (ORF-X) in the complementary strand. Introduction  
446 of two point mutations in this region to disrupt ORF-X without affecting the L amino acid sequence  
447 (Extended Data Fig. 4) finally enabled cloning of the full-length genome suggesting that ORF-X was likely  
448 toxic in bacteria.

449

450 **Recovery of recombinant MBaMV and MeV from cDNA.**

451 For the recovery of recombinant MBaMV,  $4 \times 10^5$  BSR-T7 cells were seeded in 6-well plates. The next day,  
452 the indicated amounts (written below) of antigenomic construct, helper plasmids (-N, -P and -L from  
453 measles virus), T7 construct, and LipofectamineLTX / PLUS reagent (Invitrogen) were combined in 200  
454  $\mu$ L Opti-MEM (Invitrogen). After incubation at room temperature for 30 minutes, the DNA - Lipofectamine  
455 mixture was added dropwise onto cells. The cells were incubated at 37°C for 24 hours. The cells were  
456 trypsinized and passed onto Vero-bCD150 cells ( $2.0 \times 10^6$  cells / flask in one 75cm<sup>2</sup> flask.). We collected  
457 supernatant 2 days after overlay and reamplified MBaMV in fresh Vero-bCD150 cells.

458 The amount of measles plasmids used for rescue is reported in our previous study<sup>44</sup>: 5  $\mu$ g antigenomic  
459 construct, 1.2  $\mu$ g T7-MeV-N, 1.2  $\mu$ g T7-MeV-P, 0.4  $\mu$ g T7-MeV-L, 3  $\mu$ g of a plasmid encoding a codon-  
460 optimized T7 polymerase, 5.8  $\mu$ L PLUS reagent, and 9.3  $\mu$ L Lipofectamine LTX.

461 The rescue of MeV was done exactly same way as MBaMV rescue except that 5  $\mu$ g of pEMC-IC323eGFP  
462 was used for transfection and Vero-hCD150 cells were used for coculturing.

463

464 **Titration of viruses and plaque assay**

465 For MBaMV, a monolayer of Vero-bCD150 cells in 12 well was infected by 500  $\mu$ l of serially diluted  
466 samples for 1 hour, followed by medium replacement with methylcellulose containing DMEM. 5 dpi, the  
467 number of GFP positive plaque was counted to determine titer. For the plaque assay, infected Vero-bCD150  
468 cells were incubated under methylcellulose containing DMEM for 7 days. Cells were then stained with 1%  
469 crystal violet and 1% neutral red sequentially. For MeV, we used Vero-hCD150 cells and fixed the plates at  
470 4dpi.

471

472 **Growth analysis**

473  $2.0 \times 10^5$  cells / well were seeded in 12 well plate. Cells were infected by indicated titer of viruses (MOI  
474 0.01 or 0.5) for one hour, followed by replacement of fresh medium. Viruses were grown for 5 days with  
475 medium change every day. Collected supernatants were used for titration.

476

477 **Generation of Vero-bCD150 cells and Vero-human nectin-4 cells.**

478  $4.0 \times 10^5$  of VeroCCL81 cells were transfected with 2  $\mu$ g of pCAGGS-Ig $\kappa$ -HA-bCD150-P2A-Puro with  
479 Lipofectamine 2000 (Invitrogen); cells were selected under 5  $\mu$ g/ml of puromycin (Gibco) until colonies  
480 were visible. Colonies were isolated independently and checked for HA expression using FACS. Vero-  
481 human nectin-4 cells were generated by transfecting pCAGGS-human nectin-4-P2A-Puro into VeroCCL81  
482 cells, followed by 5  $\mu$ g/ml of puromycin selection, and clone isolation. Surface expression was checked by



483 FACS.

484

485 **Generation of VSV-pseudotyped virus and entry assay.**

486 6 x 10<sup>6</sup> cells of 293T were seeded in a 10cm dish (pre-coated by poly-L-lysine (Sigma)) one day before  
487 transfection. 12 µg of RBP plus 12 µg of F coding plasmid from MeV, CDV, or MBaMV were transfected  
488 to cells by PEI MAX (polysciences). Vesicular stomatitis virus (VSV)-deltaG-Gluc supplemented by G  
489 protein (VSVΔG-G\*) were infected at MOI = 10 for one hour at 8 hours post plasmid transfection. Cells  
490 were washed with PBS three times and medium was maintained with Opti-MEM for 48 hours. Supernatant  
491 was collected and ultra-centrifuged at 25,000 rpm x 2 hours and the pellet was re-suspended with 100ul of  
492 PBS<sup>45</sup>. For the quantification of pseudotyped viral entry, CHO cells in 10cm dish were transfected with 24  
493 µg of hCD150, dCD150, or bCD150 expressing plasmid with PEI MAX. CHO cells were passaged onto  
494 96 well plates at 8 hours post transfection The pseudotyped-VSV of MeV, CDV, or MBaMV were used to  
495 infect the CHO cells. Renilla luciferase units (RLU) were measured by Renilla luciferase assay system  
496 (Promega) to quantify the pseudotype virus entry into cells.

497

498 **Image based fusion assay.**

499 CHO cells were seeded at 50,000 cells in 48-well dish 24 hours before transfection. Cells were transfected  
500 with 200 µg of pCAGSS-RBP-HA (of MeV/CDV/MBaMV), 200 µg of pCAGGS-F-AU1(of  
501 MeV/CDV/MBaMV), pCAGGS-Igκ-HA-CD150 (20 ng human, 5 ng dog, or 20 ng bat), and 50 µg of  
502 pEGFP-C1 Lifeact-EGFP (purchased from Addgene) with 2.5 µl of polyethylenimine max (polysciences).  
503 At 36 hours post transfection, cells were imaged with a Celigo imaging cytometer (Nexcelom) with the  
504 GFP channel, and pictures were exported at the resolution of 5 micrometer / pixel. The GFP-positive foci  
505 (single cell or syncytia) were analyzed by ImageJ (developed by NIH), creating the profile of individual  
506 GFP-positive foci with size information.

507 For the evaluation of syncytia size, we first filtered the GFP-positive foci with the size of  $\geq 10$  pixel<sup>2</sup>,  
508 which is the median size of GFP area in the well of MeV-F plus LifeactGFP transfection to exclude non-  
509 specific background noise. Then we calculated the frequency of syncytia which is defined as the GFP counts  
510 of  $\geq 100$  pixel<sup>2</sup> (10 times of median size of single cells) / total GFP counts of  $\geq 10$  pixel<sup>2</sup>.

511

512 **Surface expression check of bCD150 in Vero-bCD150 cells and human nectin-4 in Vero-human**  
513 **nectin-4 cells by FACS**

514 50,000 cells in a 96 well plate were dissociated with 10 µM EDTA in DPBS, followed by a 2% FBS in  
515 DPBS block. Cells were treated with primary antibody for one hour at 4°C, then washed and treated by  
516 secondary antibody for one hour at 4°C. Vero-bCD150 cells were examined with a Guava® easyCyte™

517 Flow Cytometers (Luminex) for the detection of signal. Vero-human nectin-4 cells were subjected to Attune  
518 NxT Flow Cytometer (ThermoFisher Scientific). For primary antibody, mouse monoclonal nectin-4  
519 antibody (clone N4.61, Millipore Sigma) and rabbit polyclonal HA tag antibody (Novus biologicals) were  
520 used at appropriate concentration indicated by the vendors. For secondary antibody, goat anti-rabbit IgG  
521 H&L Alexa Fluor® 647 (Abcam) and goat anti-mouse IgG H&L Alexa Fluor® 647 (Abcam) were used  
522 appropriately. FlowJo was used for analyzing FACS data and presentation.

523

#### 524 **Soluble CD150 production and purification**

525 Production and purification of soluble CD150 is as previously reported<sup>46</sup>. Soluble CD150 is a chimera  
526 comprising the human V (T25 to Y138) and mouse C2 domains (E140 to E239) + His6-tag, which was  
527 cloned into pCA7 vector. The expression plasmid was transfected by using polyethyleneimine, together  
528 with the plasmid encoding the SV40 large T antigen, into 90% confluent HEK293S cells lacking N-  
529 acetylglucosaminyltransferase I (GnTI) activity. The cells were cultured in DMEM (MP Biomedicals),  
530 supplemented with 10% FCS (Invitrogen), l-glutamine, and nonessential amino acids (GIBCO). The  
531 concentration of FCS was lowered to 2% after transfection. The His6-tagged protein was purified at 4 days  
532 post transfection from the culture media by using the Ni<sup>2+</sup>-NTA affinity column and superdex 200 GL  
533 10/300 gel filtration chromatography (Amersham Biosciences). The pH of all buffers were adjusted to 8.0.  
534 Soluble CD150 Fc fusion avitag was purchased from BPSbioscience, and reconstituted by PBS.

535

#### 536 **Macrophage experiments**

537 CD14<sup>+</sup> monocytes were isolated from leukopak purchased from the New York Blood Bank using the  
538 EasySep Human CD14 positive selection kit (StemCell #17858). For macrophage differentiation, CD14<sup>+</sup>  
539 monocytes were seeded at 10<sup>6</sup> cells/ml and cultured in R10 media (RPMI supplemented with FBS, HEPES,  
540 L-glutamine, and pen/strep) with 50 ng/ml of GM-CSF (Sigma Aldrich G5035) in a 37°C incubator. Media  
541 and cytokines were replaced 3 days post seeding. At 6 days post seeding, macrophages were infected with  
542 either MeV or MBaMV at 100,000 IU (infectious units) per 500,000 cells and were spinoculated at 1,200  
543 rpm for 1 hour at room temperature. Virus inoculum was removed and cells were incubated in R10 media  
544 with GM-CSF at 37°C. For imaging experiments, macrophages were fixed in 4% PFA at 30 hours post  
545 infection (hpi), stained with DAPI, and fluorescent and bright field images were captured on the Cytation  
546 3 plate reader. For flow cytometry experiments, infected macrophages were stained for viability at 24 hpi  
547 (LIVE/DEAD fixable stain kit from Invitrogen L34976), treated with human Fc block (BD Biosciences),  
548 stained with antibodies against CD14 (eBioscience clone 61d3) and HLA-DR (eBioscience clone LN3),  
549 fixed in 2% PFA, permeabilized with saponin, and stained for intracellular CD68 (eBioscience clone  
550 Y1/82A). Stained macrophages were run through an Attune NxT Flow Cytometer and data was analyzed

551 using FlowJo software (v10).

552

### 553 **T cell experiments**

554 PBMCs were isolated from fresh blood donations obtained through the New York Blood Center using  
555 density centrifugation and a ficoll gradient. Isolated PBMCs were then resuspended in RPMI media (10%  
556 FBS, 1% L-Glutamine, 1% Penicillin-Streptomycin) and were stimulated for T-cell activation with  
557 Concanavalin-A (ConA) at 5 ug/ml for 72 hours. Following, cells were washed once with PBS and  
558 stimulated with 10 ng/ml of IL2 for 48 hours. Cells were subsequently infected at an MOI of 0.2 with  
559 MeV, BaMV or were mock infected in 12 well plates at  $10^6$  cells/ml. Cells were collected 24 hours post  
560 infection, stained with Invitrogen's LIVE/DEAD Fixable dead cell far red dye as per the manufacturer's  
561 protocol, and were analyzed for eGFP expression by flow cytometry with an Attune NxT Flow  
562 Cytometer. Analysis was completed using FCSEXPRESS-7. A total of 2 donors were utilized for this  
563 analysis.

564

### 565 **Western blot for RBP and F protein**

566  $1 \times 10^6$  of 293T cells were seeded on to collagen coated 6 well plate. 293T cells were transfected by 2  $\mu$ g  
567 of pCAGGS, pCAGGS-MBaMV-RBP-HA, or pCAGGS-MBaMV-F-AU1 using polyethylenimine max  
568 (polysciences). Cells were washed with PBS, then lysed by RIPA buffer. Collected cytosolic proteins were  
569 run on 4 - 15% poly polyacrylamide gel (Bio-rad. #4561086) and transferred onto PVDF membrane  
570 (FisherScientific, #45-004-113), followed by primary antibody reaction and secondary antibody reaction.  
571 Rabbit polyclonal HA tag antibody (Novus biologicals, #NB600-363), rabbit polyclonal AU1 epitope  
572 antibody (Novus biologicals, #NB600-453) was used for primary antibody for HA and AU1 tag detection.  
573 Rabbit monoclonal antibody (Cell signaling technology, #2118) were chosen as primary antibody to detect  
574 GAPDH. Alexa Fluor 647-conjugated anti-rabbit antibody (Invitrogen, #A-21245) was used as secondary  
575 antibody appropriately. Image capturing were done by Chemidoc<sup>TM</sup> MP (Biorad).

576

### 577 **Transcriptome analysis of MBaMV**

578  $4.0 \times 10^5$  Vero-bCD150 cells were infected by MBaMV at MOI = 0.01. Cytosolic RNA was collected by 500  
579  $\mu$ l of Trizol (Ambion) at 2 dpi. Collected cytosolic RNA was sequenced by direct RNA sequence by  
580 MinION (Oxford Nanopore Technologies) with some modifications in the protocol. First, we started library  
581 preparation from 3  $\mu$ g of RNA. Second, we used SuperScript IV (Invitrogen) instead of SuperScript III.  
582 Sequencing was run for 48 hours by using R9.4 flow cells. The fastq file was aligned to MBaMV genome  
583 sequence by minimap2 and coverage information was extracted by IGVtools.

584

## 585 **Evaluation of P mRNA editing**

586 Infection and RNA extraction was same as above (transcriptome analysis). 1 ug RNA was reverse  
587 transcribed by TetroRT (bioline) with poly-A primer, followed by PCR with primer set of Pedit-f (sequence;  
588 GGGACCTGTTGCCCGTTTAA) and Pedit-r (sequence; TGTCGGACCTCTTACTACTAGACT).  
589 Amplicons were processed by using NEBNext Ultra DNA Library Prep kit following the manufacturer's  
590 recommendations (Illumina, San Diego, CA, USA), and sequenced by Illumina MiSeq on a 2x250 paired-  
591 end configuration at GENEWIZ, Inc (South Plainfield, NJ, USA). Base calling was conducted by the  
592 Illumina Control Software (HCS) on the Illumina instrument. The paired-end fastq files were merged by  
593 BBTools. These merged fastq files were aligned to the reference sequence using bowtie2, creating a SAM  
594 file, and we counted the number of P-editing inserts.

595

## 596 **Bat challenge experiment and evaluation of infection.**

597 Six Jamaican fruit bats (*Artibeus jamaicensis*) were inoculated with  $2 \times 10^5$  PFU MBaMV-eGFP; three bats  
598 were intranasally (I.N.) and 3 bats were intraperitoneally (I.P.). At 1 week post virus inoculation, bat was  
599 subjected to blood and serum collection, visually inspected for GFP expression around the nares, oral cavity,  
600 and eyes by LED camera in each group (I.N. and I.P.). At 2 weeks post virus infection, blood, serum, and  
601 tissues (lung, spleen, and liver) were collected from one bat in each group. At 3 weeks post virus infection,  
602 blood, serum, and tissues (lung, spleen, and liver) were collected from one bat in each group.

603 Blood RNA was extracted by Trizol. RNA was reverse transcribed by Tetro cDNA synthesis kit (Bioline)  
604 with the primer of 'GAGCAAAGACCCCAACGAGA' targeting MBaMV-GFP genome, then the number  
605 of genomes was quantified by SensiFAST™ SYBR® & Fluorescein Kit (Bioline) and CFX96 Touch Real-  
606 Time PCR Detection System (Biorad). The primer set for qPCR is 'GGGGTGCTATCAGAGGCATC' and  
607 'TAGGACCCTTGGTACCGGAG'.

608 Virus neutralization assay was done as follows. Heat inactivated (56 degrees x 30 minutes) bat serum was  
609 serially diluted by 3 times (starting from 5 times dilution) and mixed with  $2 \times 10^4$  PFU /ml of MBaMV at  
610 1: 1 ratio for 10 minutes at room temperature. 100 µl of mixture was applied to Vero-batCD150 cells in 96  
611 well. GFP foci were detected and counted by Celigo imaging cytometer (Nexcelom). GFP counts of serum  
612 treated samples were normalized by no serum treated well.

613 Tissues were fixed with 10% buffered formalin and embedded with paraffin, then thin-sliced. GFP-IHC  
614 was performed by using VENTANA DISCOVERY ULTRA. Rabbit monoclonal antibody (Cell signaling  
615 technology, #2956) was used as a primary antibody, and OMNIMap anti-rabbit-HRP (Roche, #760-4310)  
616 was used as a secondary antibody. The GFP signal was visualized by using Discovery ChromoMap DAB  
617 kit (Roche, #760-2513). Tissues were counterstained with hematoxylin to visualize the nuclei.

618

619 **In-silico docking**

620 In silico docking was performed with MOE 2018.1001 (Chemical Computing Group), as previously  
621 described<sup>30</sup>. A homology model of MBaMV L was created based on the structural coordinates of PIV5-L  
622 (PDB ID: 6V86) using the SWISS-MODEL homology modeling server<sup>47</sup>. Prior to docking, the model of  
623 the MBaMV L protein was protonated and energy minimized. An induced-fit protocol using the Amber10  
624 force field was implemented to dock ERDRP-0519 and GHP-88309 into MBaMV L. For binding of  
625 ERDRP-0519, residues Y1155, G1156, L1157, E1158, and H1288 and for binding of GHP-88309, residues  
626 E858, D863, D997, I1009, and Y1106 were pre-selected as docking targets, which are predicted to line the  
627 docking sites of ERDRP-0519 and GHP-88309, respectively, in MeV L. Top scoring docking poses were  
628 selected and aligned in Pymol to the previously characterized in silico docking poses of the inhibitors to  
629 MeV L protein. Sequence alignment of MBaMV and MeV L proteins was performed using Clustal Omega<sup>48</sup>.  
630 Conservation was scored using the AL2CO alignment conservation server<sup>49</sup>.

631

632 **Transmission electron microscopy (TEM)**

633 Routine transmission electron microscopy processing was done as described<sup>50</sup>. The Vero-bCD150 cells  
634 infected by MBaMV for 3 days were washed with phosphate-buffered saline and then fixed with 2.5%  
635 glutaraldehyde in 0.1 M sodium cacodylate buffer (pH 7.4) on ice for 1 hour. The cells were scraped off the  
636 100 mm tissue culture treated petri dish and pelleted by low-speed centrifugation (400g for 5 minutes). The  
637 pellet was fixed for 30 minutes with the same fixative before secondary fixation with 2% osmium tetroxide  
638 on ice for 1 hour. The cells were then stained with 2% uranyl aqueous solution *en bloc* for 1 hour at room  
639 temperature, dehydrated with a series of increasing ethanol gradients followed by propylene oxide  
640 treatment, and embedded in Embed 812 Resin mixture (Electron Microscopy Sciences). Blocks were cured  
641 for 48 h at 65°C and then trimmed into 70 nm ultrathin sections using a diamond knife on a Leica Ultracut  
642 6 and transferred onto 200 mesh copper grids. Sections were counterstained with 2% uranyl acetate in 70%  
643 ethanol for 3 min at room temperature and in lead citrate for 3 minutes at room temperature, and then  
644 examined with a JEOL JSM 1400 transmission electron microscope equipped with two CCD camera for  
645 digital image acquisition: Veleta 2K x 2K and Quemesa 11 megapixel (EMSIS, Germany) operated at 100  
646 kV.

647

648 **Ethics declaration.**

649 Animal study was performed following the Guide for the Care and Use of Laboratory Animals. Animal  
650 experiment was approved by the Institutional Animal Care and Use Committee of Colorado State University  
651 (protocol number 1090) in advance and conducted in compliance with the Association for the Assessment  
652 and Accreditation of Laboratory Animal Care guidelines, National Institutes of Health regulations,

653 Colorado State University policy, and local, state and federal laws.

654

### 655 **Human subjects research**

656 Normal primary dendritic cells and macrophages used in this project were sourced from ‘human peripheral  
657 blood Leukopack, fresh’ which is provided by the commercial provider New York Blood center, inc.  
658 Leukapheresis was performed on normal donors using Institutional Review Board (IRB)-approved consent  
659 forms and protocols by the vendor. The vendor holds the donor consents and the legal authorization that  
660 should give permission for all research use. The vendor is not involved in the study design and has no role  
661 in this project. Samples were deidentified by the vendor and provided to us. To protect the privacy of donors,  
662 the vendor doesn’t disclose any donor records. If used for research purposes only, the donor consent applies.

663

### 664 **Data and materials availability:**

665 The raw next generation sequencing results of bat surveillance, P gene editing, and transcriptome by  
666 MinION are uploaded at NCBI GEO: GSE166170, GSE166158, and GSE166172, respectively.

667

668 Assembled MBaMV sequence and pEMC-MBaMVeGFP sequence information are available at  
669 MW557651 and MW553715, respectively. Cytochrome oxidase I host sequence and cytochrome b host  
670 sequence of virus infected bat are available at MW554523 and MW557650. MeV genomic cDNA coding  
671 plasmid (pEMC-IC323eGFP) sequence is available at NCBI Genbank: MW401770.

672

### 673 **Authors contributions**

674 SI, SJA and BL conceived this study. SI conducted fusion assay, rescuing viruses, growth analysis, RNA  
675 sequencing of transcriptome analysis, and generation of cell lines written in the study. RLF conducted TEM  
676 imaging. JCC, JA, AP, and JL performed the macrophage and T cell experiments and data analysis. KYO  
677 conducted VSV-pseudotype entry assay. RMC and PKP provided ERDRP-0519 and GHP-88309 in addition  
678 to *in silico* modelling of MBaMV-L. HPC evaluated protein production by Western blot. TH provided  
679 structure-guided insights into conservation of RBP and CD150 binding as well as soluble human CD150  
680 for inhibition assay. KYO and SK evaluated surface expression of morbillivirus receptors. CSS evaluated  
681 P-mRNA editing frequency from NGS data. TS, ME, SZ performed bat challenge experiment. ED  
682 conducted bat surveillance in collaboration with JEE and PD. SJA and HW conducted NGS analysis of bat  
683 surveillance and retrieved MBaMV sequences. JEE, PD and SJA provided insights into viral ecology and  
684 zoonotic threats. BL supervised this study. SI, JCC, SJA, and BL wrote the manuscript.

685

### 686 **Acknowledgements**

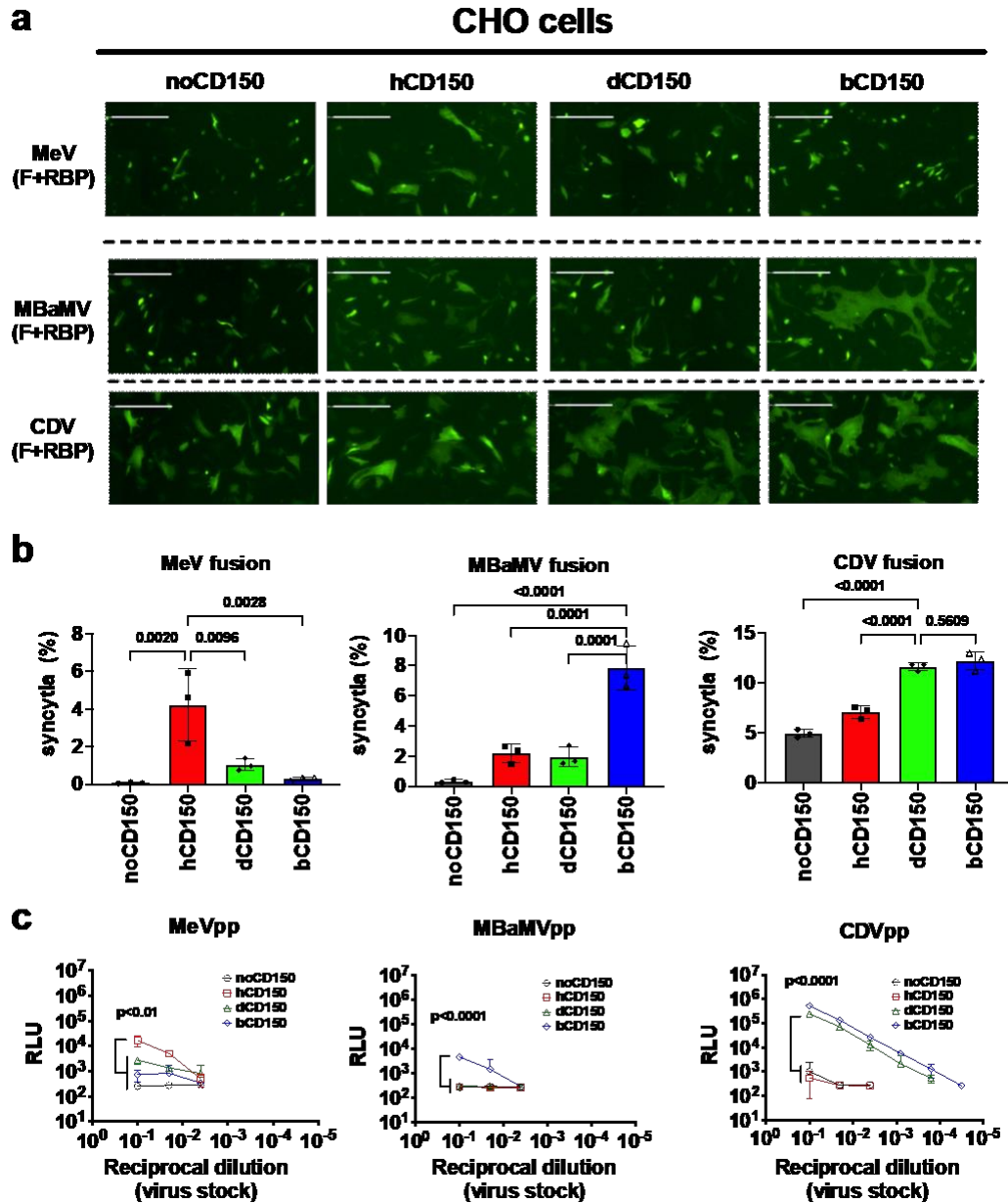
687 S.I. was supported by Fukuoka University's Clinical Hematology and Oncology Study Group (CHOT-SG).  
688 This study was supported in part by NIH grants AI123449 (B.L.), AI071002 (R.K.P and B.L.), AI149033  
689 (B.L. and J.L.), USAID PREDICT (S.J.A, J.E.E., P.D., E.D.). J.C.C. J.A., K.Y.O, A.P., C.S.S.  
690 acknowledges support from T32 AI07647. K.Y.O. was additionally supported by F31 (AI154739). This  
691 work was also supported by Japan Agent for Medical Research and Development (AMED) Grant  
692 20wm0325002h, JSPS KAKENHI Grant Numbers 20H03497 and Joint Usage/Research Center program  
693 of Institute for Frontier Life and Medical Sciences, Kyoto University (T.H.).

694

695

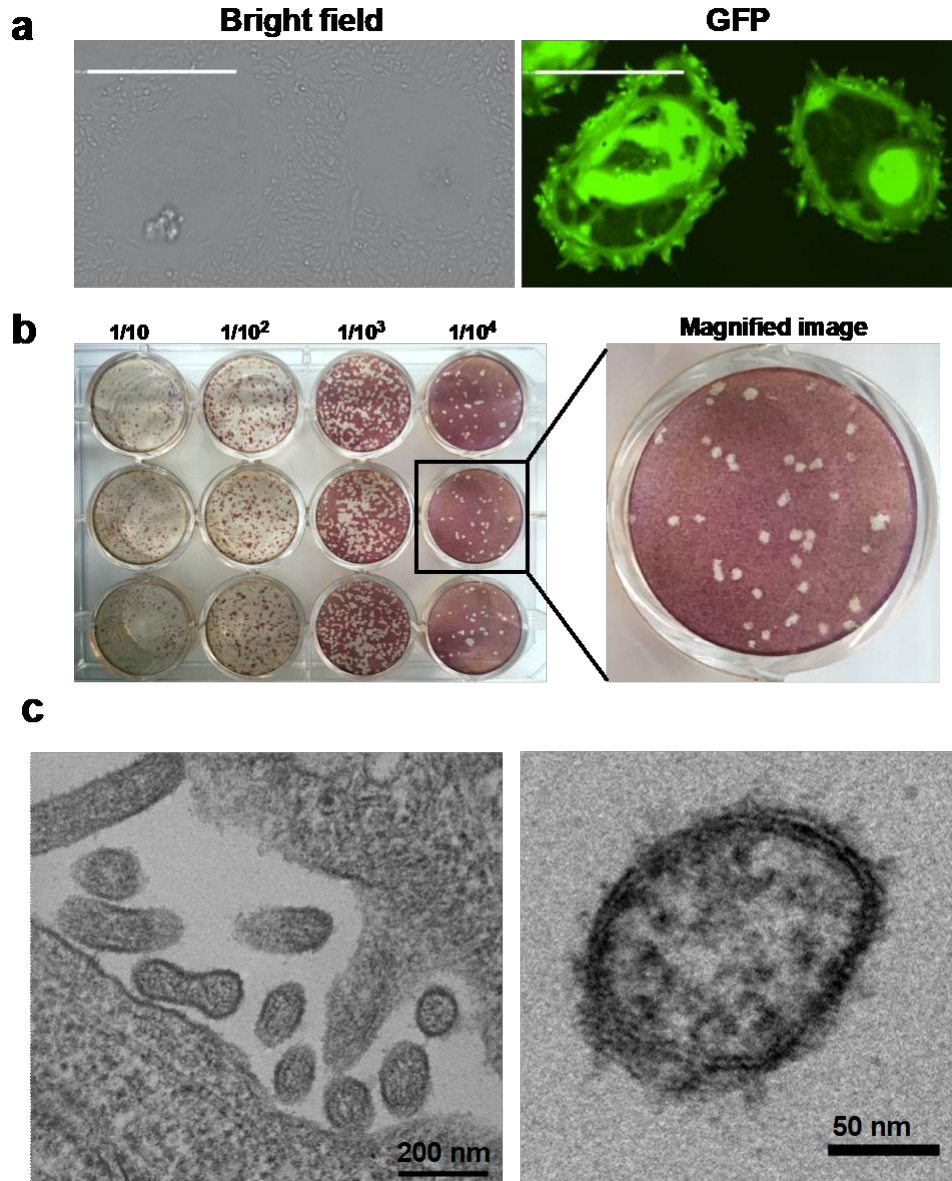
696

697



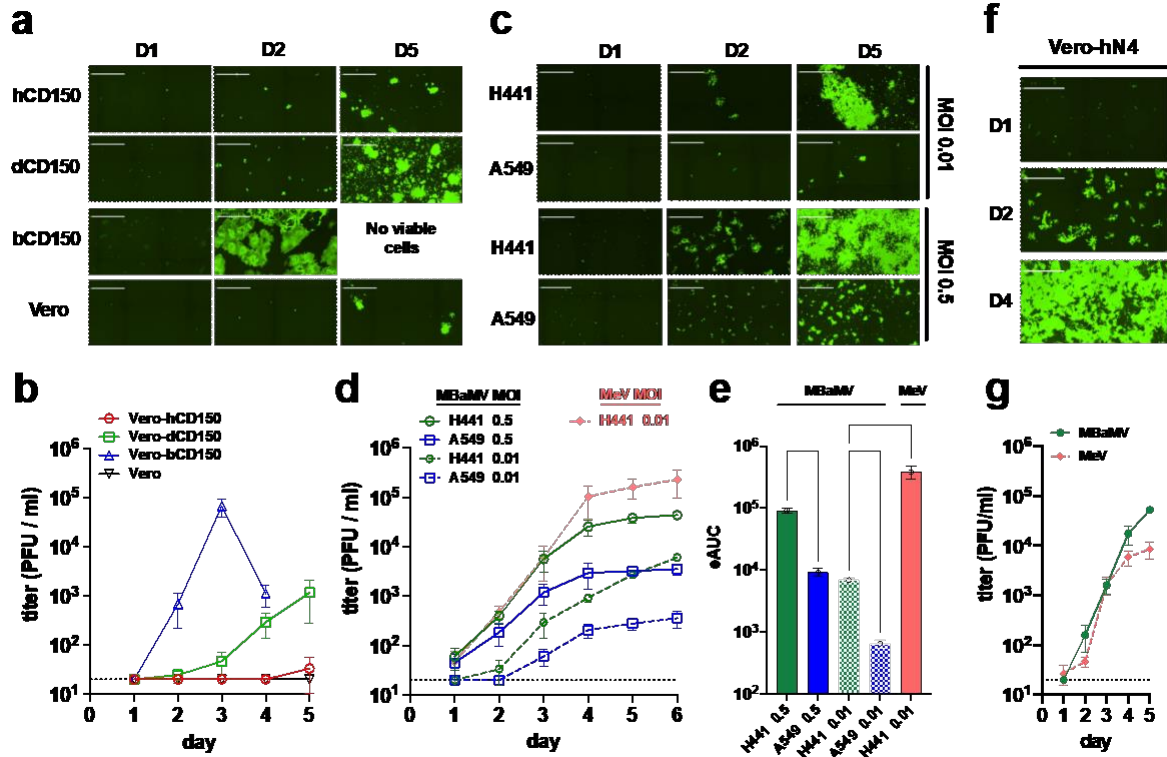
698  
 699 **Figure 1. MBaMV envelope glycoproteins use host specific CD150 (SLAMF1) for fusion and entry.**  
 700 **a**, Syncytia formation in CHO cells co-transfected with the indicated morbillivirus envelope glycoproteins,  
 701 species-specific CD150, and Life-act-GFP. Images were taken by the Celigo Imaging Cytometer  
 702 (Nexcelom) at 48 hours post-transfection (hpt) and are computational composites from an identical number  
 703 of fields in each well. White bar equals 200 micrometers. Brightness and contrast settings were identical.  
 704 **b**, Quantification of syncytia formation in (a) (see methods). Data are mean +/- S.D. from 3 independent  
 705 experiments. Indicated adjusted p values are from ordinary one-way ANOVA with Dunnett's multiple  
 706 comparisons test. **c**, VSV-pseudo particle (pp) entry assay showed similar trends. Adjusted p values  
 707 obtained as in (b) but only for comparing groups at the highest viral inoculum used (10<sup>-1</sup> reciprocal dilution).





708  
709

710 **Figure 2. Virological characterization of myotis bat morbillivirus (MBaMV).** **a**, Syncytia formation in  
711 Vero-bCD150 cells induced by MBaMV 3 days post-infection (dpi). Cells formed syncytia involving > 100  
712 nuclei upon infection (bright field), which is clearly outlined by virus expressed GFP (right). Scale bar  
713 equals 500 micrometers. **b**, MBaMV plaque formation in Vero-bCD150 cells. Cells were infected by 10-  
714 fold serially diluted virus stock, incubated with methylcellulose containing-DMEM and stained with crystal  
715 violet and neutral red 7 dpi. Diameter of well is 22 mm. One well is magnified to show the plaque  
716 morphology in detail. **c**, shows transmission electron microscopy (TEM) images of MBaMV virion on the  
717 surface of Vero-bCD150 cells at 3 dpi. Numerous enveloped virions are budding from the plasma membrane  
718 (left). Magnified image (right) shows virion and ribonucleoprotein complex (RNP).



719

720

721

722

723

724

725

726

727

728

729

730

731

732

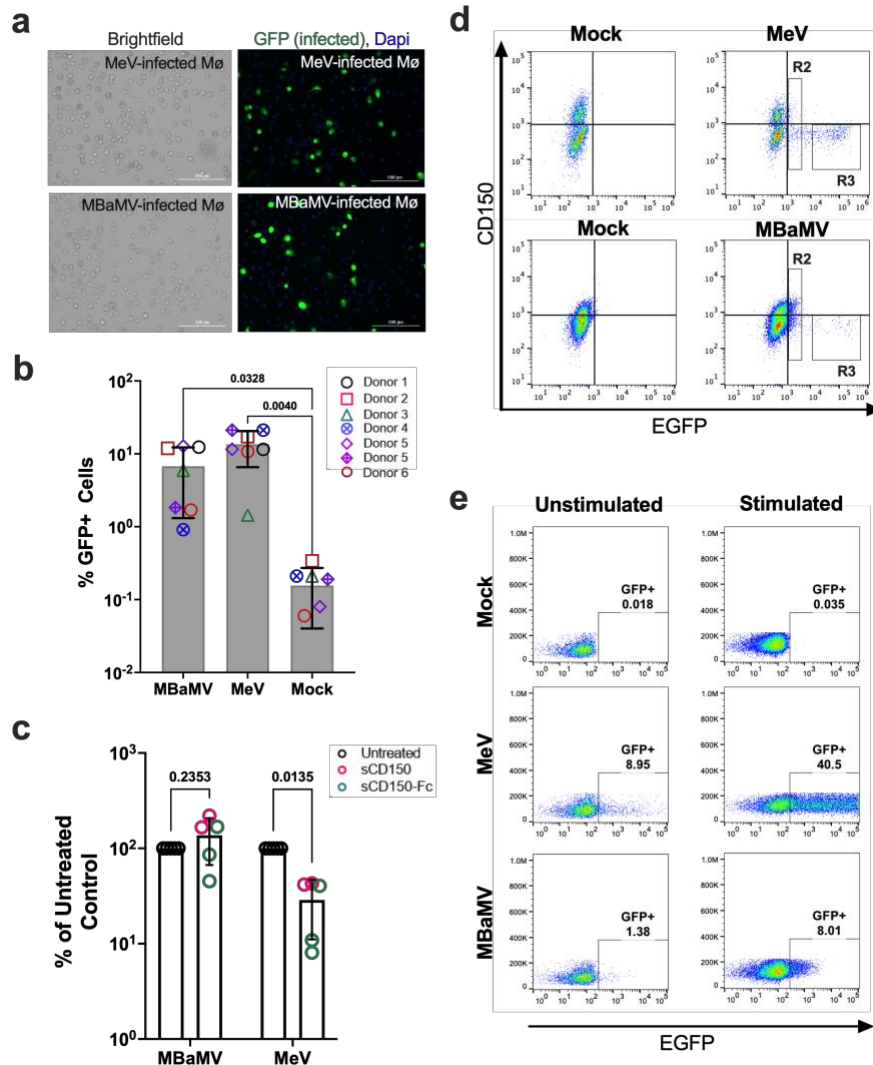
733

734

735

736

**Figure 3. MBaMV replicates efficiently in cells expressing bCD150 and human nectin-4.** **a-b**, Vero-hCD150, Vero-dCD150, Vero-bCD150, and Vero cells were infected with rMBaMV-EGFP (MOI 0.01). Virus replication and spread were monitored by imaging cytometry (**a**) and virus titer in the supernatant (**b**). **a**, Large syncytia were evident in Vero-bCD150 cells by 2 dpi. **b**, Supernatant was collected every day and the virus titer was determined by a GFP plaque assay (see methods). Data shown are mean  $\pm$  S.D. from triplicate experiments. **c-e**, H441 and A549 cells were infected with rMBaMV-EGFP at a low (0.01) or high (0.5) MOI. Virus replication and spread were monitored as in **a-b**. **c**, Infected H441 and A549 cells at 1, 2 and 5 dpi (D1, D2, D5). **d**, Virus growth curves represented by daily titers in the indicated conditions. Data shown are mean titers  $\pm$  S.D. from triplicate infections. **e**, The empirical Area Under Curve (eAUC) was obtained from each growth curve and plotted as a bar graph (mean  $\pm$  S.D.) (PRISM v 9.0). Adjusted p values are indicated (one-way ANOVA Dunnett's T3 multiple comparison test). **f-g**, Vero-human nectin-4 cells (Vero-N4) were infected with MBaMV and MeV (MOI 0.01). **f**, MBaMV infected Vero-hN4 at D1, D2 and D4. **g**, Replicative virus titers for MBaMV and MeV on Vero-hN4 cells over 5 days (mean  $\pm$  S.D., n=3). White bar in **a**, **c**, and **f** equals 1 millimeter. All images shown are captured by a Celigo Imaging Cytometer (Nexcelom). Images are computational composites from an identical number of fields in each well. The limit of detection for virus titer determination is 20 PFU/ml and is indicated by the dotted line in **b**, **d**, and **g**.



737  
738 **Figure 4. MBaMV infects human monocyte-derived macrophages (MDM) in a CD150-independent**  
739 **manner. a-b,** MDMs were infected with EGFP-reporter MeV or MBaMV ( $1 \times 10^5$  IU/sample) and were  
740 either (a) fixed by 2% PFA at 24 hpi, DAPI-stained and imaged (scale bar is 200  $\mu$ m), or (b) quantified by  
741 flow cytometry. The percent of CD68+GFP+ MDMs from 6 donors are shown. Open and crossed symbols  
742 indicate experiments using lot 1 and lot 2 viruses, respectively. Adjusted p values are from one way ANOVA  
743 with Dunnett's multiple comparisons test. **c,** Soluble human CD150 (sCD150) or a dimeric Fc fusion  
744 construct (sCD150-Fc) inhibited MeV but not MBaMV infection of macrophages. GFP+ events in untreated  
745 controls were set to 100%, and entry under sCD150/sCD150-Fc were normalized to untreated controls.  
746 Adjusted p values are from two-way ANOVA with Šidák's multiple comparisons test. In (b) and (c), data  
747 shown are mean  $\pm$  S.D. from multiple experiments (N=5-7) with individual values also shown. (d)  
748 Exemplar FACS plots from the summary data shown in (b). R2 (GFP-dim) and R3 (GFP-bright/CD150-  
749 low) gates are indicated as described in the text. **e,** ConA/IL-2 stimulated PBMCs were infected with MeV  
750 or MBaMV (MOI of 0.1) and analyzed for GFP expression by flow cytometry at 24 hpi